Reversing and Nonreversing Heat Capacity of Poly(lactic acid) in the Glass Transition Region by TMDSC

M. Pyda*,†,§ and B. Wunderlich†,‡

Department of Chemistry, The University of Tennessee, Knoxville, Tennessee 37996-1600 USA; Chemical Sciences Division, Oak Ridge National Laboratory, Oak Ridge, Tennessee 37831 USA; and Department of Chemistry, The University of Technology, Rzeszow, 35959 Rzeszow, Poland

Received July 22, 2005; Revised Manuscript Received October 14, 2005

ABSTRACT: A study of the glass transition of an amorphous and a semicrystalline poly(lactic acid) (PLA) is performed with adiabatic calorimetry, differential scanning calorimetry (DSC), and temperature-modulated DSC (TMDSC). The reversing, total, and nonreversing apparent heat capacities of samples with different contents of L- and D-lactic acid and with various thermal histories were evaluated. Different modes of TMDSC analyses of amorphous and semicrystalline PLA were compared to the total heat capacity from standard DSC. The enthalpy relaxation and the cold crystallization in the glass transition region are largely irreversible. The melting is largely irreversible, but a 100% reversing fraction is observed at low temperatures from 375 to 420 K, which becomes small inside the major melting peak at about 440 K. From the TMDSC of amorphous PLA, the combined information on endothermic and exothermic enthalpy relaxation and glass transition were deconvoluted into the reversing and nonreversing components. The glass transition temperature from the reversing heat capacity and the enthalpy relaxation peaks from the nonreversing component shift to higher temperature for increasingly annealed PLA. The relaxation times for aging decrease on cooling until the glass transition is reached and then increase. This behavior is linked to cooperativity. All quantitative thermal analyses are based on the heat capacity of the solid and liquid, evaluated earlier with the advanced thermal analysis system (ATHAS).

1. Introduction

Understanding of the thermodynamic properties of macromolecules, such as the biodegradable poly(lactic acid) (PLA), requires quantitative thermal analysis *and* interpretation of the underlying molecular motion.[1,2] The PLA is a biocompatible and bioabsorbable thermoplastic polymer, available for fiber, film, and bulk applications.[3−6] It can be amorphous or semicrystalline, characterized by a weight fraction crystallinity, w_c, depending on stereochemical structure and thermal history. According to the chemical structure of the repeating unit, $[C^*HCH_3-COO-]_x$, L- and D-stereoisomers are possible and can yield the two corresponding pure homopolymers and a large series of regular to random copolymers. Commonly the PLAs are based on biological sources which contain the L-isomer. In our study two samples of poly(L-lactic acid) with different amounts of D-lactic acid (1.5% and 16.4%) were used. The sample with a larger amount of D-isomer is normally fully amorphous and has been used for the investigation of the glass transition. The PLA with only 1.5% of D-isomer is usually semicrystalline and shows both a melting and a glass transition. In an early study of PLA it was suggested that the equilibrium melting temperature, T_m^o, for the L-structure is from 480 to 490 K[2,7,8] and higher for the regular stereocomplex DL-structure (493−503 K).[8] The heat of fusion for 100% crystalline was estimated in the literature[2,9,10] to be between 6.55 and 10.2 kJ mol^{-1} for L-PLA and the stereocomplex, respectively. Thermal properties of PLA have been reported earlier, but often only in the form of qualitative analyses.[11−13] Only in few cases have quantitative thermal analysis methods been applied.[2,14,15]

The thermal analysis of amorphous polymers is often complicated by irreversible effects in the temperature range of the glass transition.[16] Annealing can cause endothermic or exothermic enthalpy relaxations in the vicinity of the glass transition when the sample can approach the more stable liquid. The endothermic relaxation is called *hysteresis* and the exothermic relaxation, *aging*. A hysteresis occurs at higher temperature where a glass is superheated, so that its enthalpy is lower than that of the equilibrium liquid. Aging of glasses always occurs from the temperature of the beginning of the glass transition on cooling and becomes negligible when the glass is fully arrested, usually some 20−50 K below the glass transition temperature, T_g. The T_g of fully amorphous PLA is ca. 330 K with variations being caused by different thermal histories and stereospecificities. The glass transition, when analyzed by calorimetry on cooling, is observed as a decrease in heat capacity, C_p, which is proportional to the amount of material changing from the liquid to the solid state. A stress across interfaces to more rigid phases causes broadening and shifts of the glass transition to higher temperature and may even produce a separate rigid amorphous phase (RAF).[17] The T_g, apparent C_p, and enthalpy relaxation in the glass transition region depend on rate of change of temperature, amount of aging, and, for TMDSC, the frequency of modulation. The kinetic effects in the glass transition region have been reviewed recently.[16,18,19] The C_p of PLA for the proper baselines of the solid and liquid C_p for the discussion of phase transitions has already been established using the advanced thermal analysis system (ATHAS).[2,20,21] The solid C_p at sufficiently low temperature is based only on the atomic vibrational motion which is described

† The University of Tennessee.
‡ Oak Ridge National Laboratory.
§ The University of Technology.
* Corresponding author. E-mail: mpyda@utk.edu.

10.1021/ma051611k CCC: $30.25
Published on Web 11/12/2005

well in the literature.[1,2,16,20] A full description of the liquid C_p based on vibrational and large-amplitude (mostly conformational) motion is known for several synthetic macromolecules[22] and also biopolymers in the presence and absence of water.[23−25]

The glass transitions involve the freezing of the cooperative, large-amplitude motion beyond the vibrational C_p and can be analyzed by modern calorimetry. Data from temperature-modulated differential scanning calorimetry (TMDSC)[16,18,26] and standard differential scanning calorimetry (DSC)[1,16] can be combined to obtain the apparent total, reversing, and nonreversing heat capacities, as was done earlier for amorphous polystyrene and poly(ethylene terephthalate).[27−31] In this paper, semicrystalline and glassy poly(lactic acid) with different thermal histories are studied with TMDSC and DSC in order to identify, separate, and describe the thermodynamics and kinetics processes.

2. Experimental Details

2.1. Samples. Poly(lactic acid), PLA, with low (1.5%, PLA-*L*) and high stereochemical D-isomer (16.4%, PLA-*H*) was obtained from Cargill Dow LLD, Chem. Co. The molecular masses of these polymers were controlled to be similar, the weight-average molar mass (M_w) being 180 000−220 000 Da. The PLA-*H* was selected to study the glass transition region due to its amorphous nature, and PLA-*L* was selected to examine the glass transition of a semicrystalline poly(lactic acid).

For C_p measurements by standard DSC, samples of 10−15 mg were used. For temperature-modulated calorimetry the sample weights were 4−10 mg. The samples for DSC and TMDSC were analyzed in sealed aluminum pans of about 24 mg.

Temperature calibrations were carried out at the phase transitions of indium (429.75 K), water (273.15 K), and tin (505.08 K). For C_p calibration, single-crystalline sapphire (Al_2O_3) was utilized for both DSC and TMDSC at each temperature of measurement.

2.2. Measurements and Instrumentation. The Q1000 calorimeter from TA Instruments, Inc., equipped with a refrigerator was used to obtain the apparent total, reversing, and nonreversing heat capacities. This calorimeter is of the isoperibol, heat-flux type. The experiments were performed in three modes: (1) standard TMDSC, with a modulation amplitude of 0.5 K and periods of either 60 or 100 s and an underlying heating rate of 1 K min^{-1}; (2) quasi-isothermal TMDSC, where the underlying heating rate is zero, and the modulation is carried out at a series of fixed temperatures, T_0, with measurements extending from 10 min to 10 h at each temperature; (3) standard DSC with different cooling and heating rates.

To obtain amorphous PLA-*H* with different thermal histories on nonisothermal aging, the samples were cooled within the calorimeter from 303 to 183 K, far enough below the glass transition to yield a metastable sample. The cooling rates were varied from 20 to 0.1 K min^{-1}. The metastable samples were then reheated at 10 K min^{-1} in the standard DSC mode and in the standard TMDSC mode. For isothermal aging, the PLA-*H* was kept at 323 K, below T_g, for 20 min to 100 h. Following this aging, the samples were analyzed by standard TMDSC.

To obtain semicrystalline samples, PLA-*L* was cooled from the melt at constant rates inside the calorimeter. A higher w_c was obtained by isothermal crystallization at $T = 418$ K for 15 h. Amorphous PLA-*L* could also be produced by quenching inside the calorimeter. Completely amorphous PLA-*L* resulted on cooling at 10 K min^{-1} or faster. The sample of PLA-*H* is inherently an amorphous sample due to its random copolymerization.

2.3. Quantitative DSC. For the quantitative DSC, three runs were carried out: one with empty reference and sample pans, to correct for asymmetry of the DSC, one with an empty reference pan and a pan filled with sapphire for calibration, and one with an empty pan and a pan filled with the sample. After steady state was obtained, the C_p was determined from the following equation:[16]

$$mc_p = K\frac{\Delta T}{q} + C_s\frac{d\Delta T}{dT_s} \quad (1)$$

where K is determined as a function of temperature from the sapphire calibration, ΔT is the temperature difference between reference and sample, proportional to the heat-flow rate, HF; C_s is the C_p of the sample calorimeter including sample and aluminum pan, and T_s is the sample temperature. The second part of eq 1 was estimated to account for about 1% of the total C_p. The accuracy of the measurements is estimated to be ±3% or better. The resulting C_ps were internally calibrated to the baselines from the ATHAS Data Bank [2,20,21] for the glass and liquid.

2.4. Quantitative TMDSC. The TMDSC results consist of the apparent total and reversing C_p.[18,26] The modulation of $T_s(t)$ with amplitude A_{T_s} and period p ($\omega = 2\pi/p$) is given by[32,33]

$$T_s(t) = T_0 + \langle q\rangle t - \langle q\rangle\frac{C_s}{K} + A_{T_s}\sin(\omega t - \epsilon) \quad (2)$$

where T_0 is the starting temperature and $\langle q\rangle$ is the underlying heating rate, obtained by forming a sliding average over a complete modulation cycle. The phase shift is ϵ, taken relative to some internal reference frequency, and C_s is the C_p of the sample calorimeter. For quasi-isothermal measurements, the underlying heating rate $\langle q\rangle$ is equal zero, and the range of interest is covered by successive runs at different values of T_0. The apparent reversing C_p is expressed by

$$C_p(\text{reversing}) = \sqrt{C_{rel}^{\ 2} + C_{im}^{\ 2}} = \frac{\langle A_\Phi\rangle}{\langle A_{T_S}\rangle\omega}K(\omega);$$
$$K(\omega) = \sqrt{1 + \tau^2\omega^2} \quad (3)$$

where C_p(reversing) is the modulus of the complex C_p, with its real, C_{rel}, and imaginary, C_{im}, parts; K is the Newton's law constant; $\langle A_\Phi\rangle$ is the heat-flow-rate amplitude, smoothed over one modulation cycle; $\langle A_{T_s}\rangle$ is the similarly smoothed modulation amplitude of T_s; and $K(\omega)$ is a frequency-dependent calibration factor with τ being a correction used when analyzing the C_p at a different frequency than the calibration. Under the usual conditions of continued linearity and stationarity, τ is a constant (= C_r/K), where C_r is the C_p of the empty reference pan and K is the constant, as before.[34−36] The C_p(reversing) was obtained from a Fourier deconvolution of the first harmonics with the TA Instruments software. It must, however, be noted that within the glass transition a contribution to C_p(reversing) also comes from higher harmonics produced by the slow sample response. Another contribution is observed from a shift in the frequency of the heat-flow rate due to interaction of $\langle q\rangle$ and ω. Finally, the slow sample response produces also a small, constant, reversible C_p contribution, which the deconvolution erroneously eliminates from the reversing C_p. All these errors are small and neglected in this discussion but could be calculated from the measured first harmonic with a simple model of the kinetics of the glass transition.[37]

3. Results

3.1. Qualitative and Quantitative DSC. Qualitative DSC traces of the heat-flow rate vs temperature for amorphous PLA-*H* and semicrystalline PLA-*L* are illustrated in Figure 1. Both the amorphous PLA-*H* and the semicrystalline PLA-*L* were analyzed after isothermal conditioning at 418 K (145 °C) for 15 h from the melt, cooling, and then reheating at 20 K min^{-1} by standard DSC. In Figure 2 the data of Figure 1 are

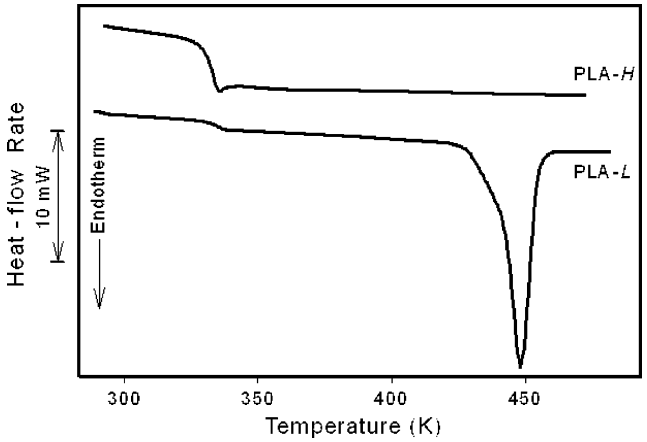

Figure 1. Experimental heat-flow rate of PLA-*H* and PLA-*L* by standard DSC. Both PLA-*L* and PLA-*H* were isothermally annealed at 418 K for 15 h, cooled, and then heated at 20 K min^{-1}.

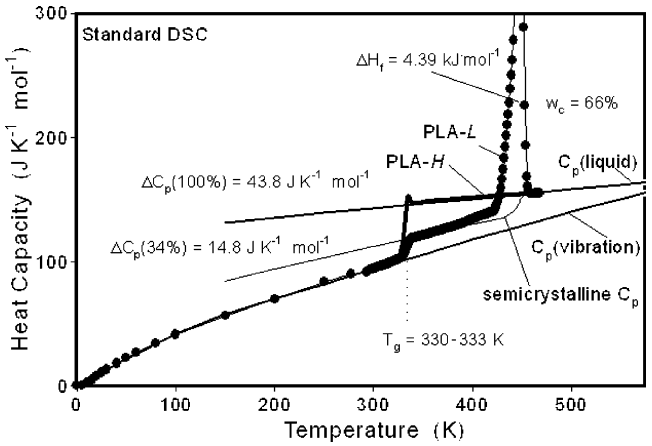

Figure 2. Quantitative evaluation of Figure 1. Additional low-temperature C_p by adiabatic calorimetry are plotted, and the ATHAS Data Bank C_p(vibrational) and C_p(liquid) is indicated. The semicrystalline C_p is derived from the heat of fusion.

quantified as apparent C_p(total), plotted together with low-temperature C_p from adiabatic calorimetry. [2] The glass transitions are at 330−333 K. The baselines C_p(vibration) and C_p(liquid) quantitatively separate nonequilibrium from equilibrium. For example, using these baseline C_ps, the change of C_p at the glass transition for the amorphous sample is 43.8 J K^{-1} mol^{-1} and for the semicrystalline PLA-*L* is 14.8 J K^{-1} mol^{-1} (34% amorphous and 66% crystalline).[2] The w_c was determined from the heat of fusion as the area above the indicated baseline.

3.2. Standard and Quasi-Isothermal TMDSC. Figure 3 shows the C_p(reversing) from quasi-isothermal TMDSC of amorphous PLA-*H* between the limits of C_p(vibration) and C_p(liquid). Good agreement between the baselines and C_p(reversing) is seen. The small hysteresis peak contributing to the total C_p in Figures 1 and 2 does not contribute to C_p(reversing).

Figure 4 reveals more details using several modes of TMDSC. The C_p(reversing) measured quasi-isothermally is different from C_p(reversing) by standard TMDSC on heating and cooling. The three results cross at a unique temperature. More detailed TMDSC are described in section 3.3.

Figure 5 contains a comparison of C_p(reversing) of amorphous PLA-*H*, semicrystalline PLA-*L*, and initially amorphous PLA-*L* by quasi-isothermal TMDSC with the

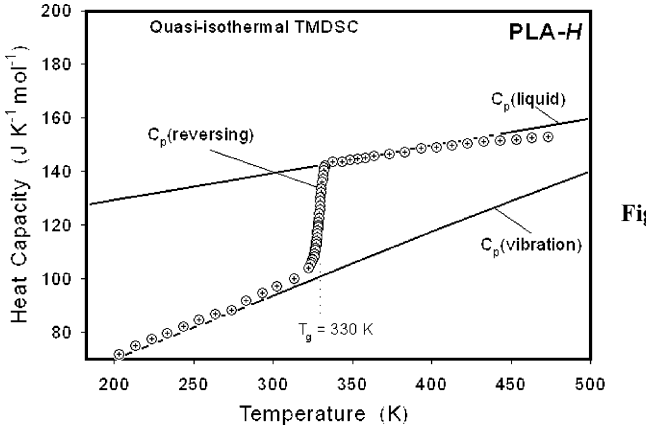

Figure 3. Reversing C_p of amorphous PLA-*H* by quasi-isothermal TMDSC in the glass transition region (amplitude of modulation 0.5 K and period, 100 s).

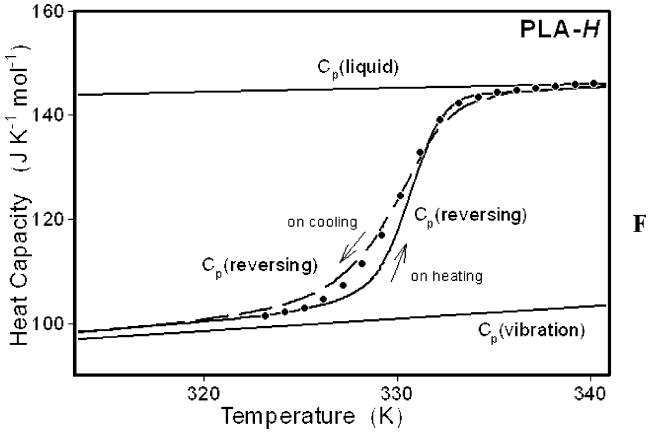

Figure 4. Comparison of C_p(reversing) of amorphous PLA-*H* from quasi-isothermal (filled circles) and standard TMDSC in the glass transition region ($\langle q \rangle = 0$ and ± 0.5 K min^{-1}, respectively, $p = 60$ s, and $A_{T_s} = 0.5$ K).

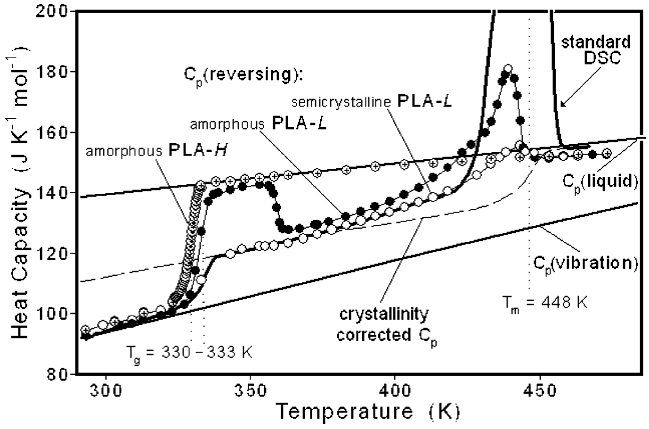

Figure 5. Comparison of C_p(reversing) of semicrystalline and amorphous PLA-*L* and of amorphous PLA-*H*, all measured by quasi-isothermal TMDSC to C_p(vibrational), C_p(liquid), and the crystallinity-corrected C_p and also the standard DSC of the semicrystalline PLA-*L* of Figure 2.

total C_p of semicrystalline PLA-*L* by standard DSC. A further comparison of the initially amorphous PLA-*L* by quasi-isothermal TMDSC with the standard DSC of the same samples heated at two different rates is given in Figure 6. The hysteresis in the glass transition region and the cold crystallization, annealing, and recrystallization above T_g are separated from C_p(reversing) under the given conditions, while in the melting range

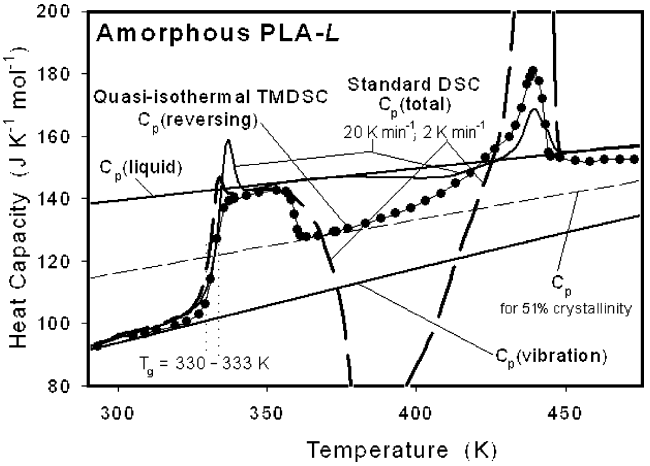

Figure 6. Comparison of C_p(reversing) of amorphous PLA-*L* by quasi-isothermal TMDSC with the C_p from standard DSC measured at heating rates of 20 and 2 K min^{-1} in the frame of the vibrational, liquid, and 51% crystalline C_p.

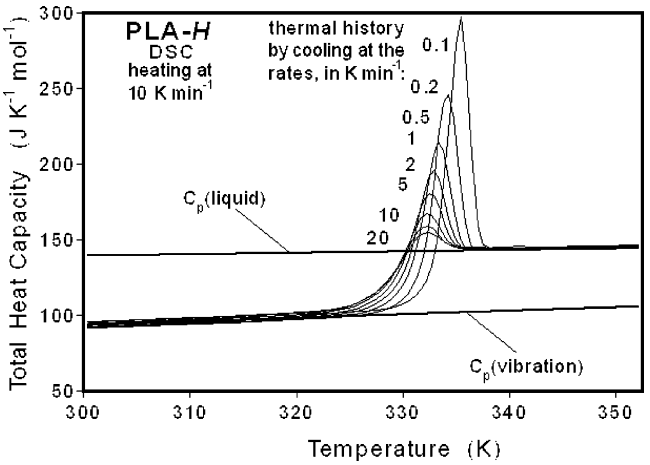

Figure 7. Total C_p of PLA-*H* with different thermal histories measured by standard DSC on heating at 10 K min^{-1} in the glass transition region.

C_p(reversing) indicates some "reversible melting".[17]

3.3. Aging and Kinetics of the Glass Transition of Amorphous PLA-*H*. In Figure 7, the changes of the apparent C_p of PLA-*H* are presented as obtained from standard DSC at the indicated cooling rates after cooling from the melt to a temperature below T_g. The apparent C_p results from an overlapping enthalpy relaxation and the C_p of the glass transition. To separate the two contributions, standard TMDSC with an underlying heating rate of 1.0 K min^{-1} was chosen slower than in Figure 7 to have less interference of the two time scales.

Parts a, b, and c of Figure 8 display the TMDSC results as total, reversing, and nonreversing C_p, respectively, where C_p(nonreversing) is the difference C_p(total) − C_p(reversing), not an independent measurement. The thermal histories created by cooling at different rates from 373 to 283 K (100 to 10 °C) were evaluated on heating. The results illustrate the overlap of nonreversing enthalpy relaxations with C_p(reversing) on heating through the glass transition. Note that both C_p(reversing) and C_p(nonreversing) change with thermal history. The C_p(reversing) has a narrower transition range with increasing in T_g when annealed, while C_p(nonreversing) documents the increasing hysteresis. The total C_p found from TMDSC is similar, but not identical, in appearance to the standard DSC in Figure 7. The peaks by DSC

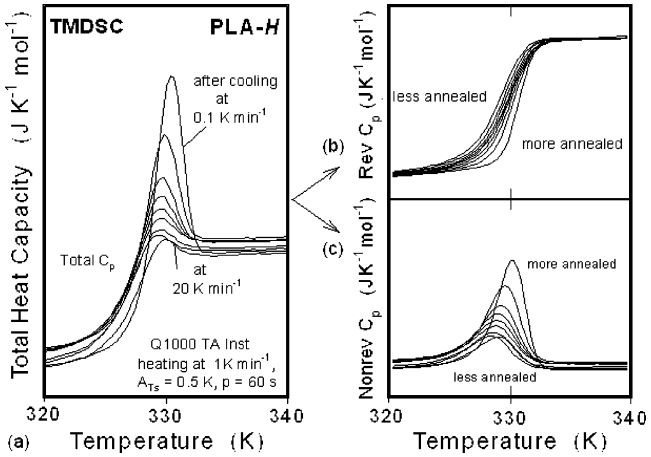

Figure 8. (a) Total, (b) reversing, and (c) nonreversing C_p of PLA-*H* with different thermal histories by TMDSC in the glass transition region on heating with $\langle q \rangle = 1$ K min^{-1}, $p = 60$ s, and $A_{T_s} = 0.5$ K.

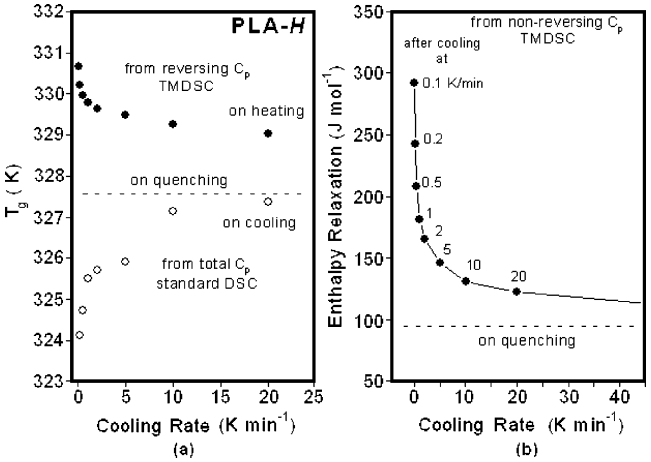

Figure 9. Changes of T_g (a) and enthalpy relaxation (b) for the analyses of PLA-*H* in Figures 7 and 8.

and TMDSC shift first to lower and then to higher temperatures for more aged PLA-*H*. This reversal of the change in peak temperature is likely caused by additional aging of the more quickly cooled samples on slower heating. A shallow exotherm of aging can also be discerned from an enthalpy plot, gained by integrating of C_p(total). The enthalpy decreases first below the enthalpy found on cooling before approaching equilibrium liquid after completion of the hysteresis.

The analysis of the data of Figures 7 and 8 is illustrated in Figure 9a,b. The T_g from Figure 8b increases with decreasing cooling rates and is presented in Figure 9a by the filled circles. For comparison, T_g by standard DSC on cooling is given by the series of open circles at the bottom of Figure 9a. The dashed line shows the highest T_g seen on cooling inside the DSC at ca. 100 K min^{-1}. A changing gap in T_g exists between DSC on cooling and TMDSC on heating after cooling with the same rate. The final gap at high cooling rates of 1.0 K again points to the additional aging which occurs on heating at 1.0 K min^{-1} for TMDSC, also affecting the peak temperature in Figure 8a,c, as stated above. The enthalpy relaxation in Figure 9b was evaluated as the integral of C_p(nonreversing) in Figure 8c. The enthalpy relaxation does not reach zero for the quenched sample, again an indication of aging on heating, reducing the measured hysteresis. The changes in Figure 9 of both T_g and enthalpy are exponential.

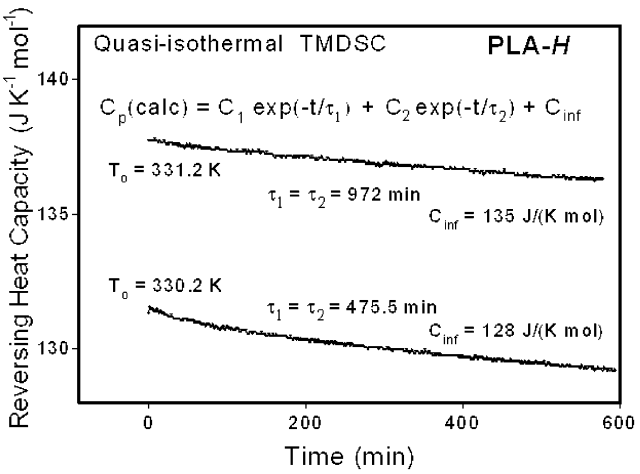

Figure 10. Examples of C_p(reversing) of PLA-*H* by quasi-isothermal TMDSC in the time domain after quenching to the indicated T_0 from 373 K (p = 60 s, and A_{T_s} = 0.5 K).

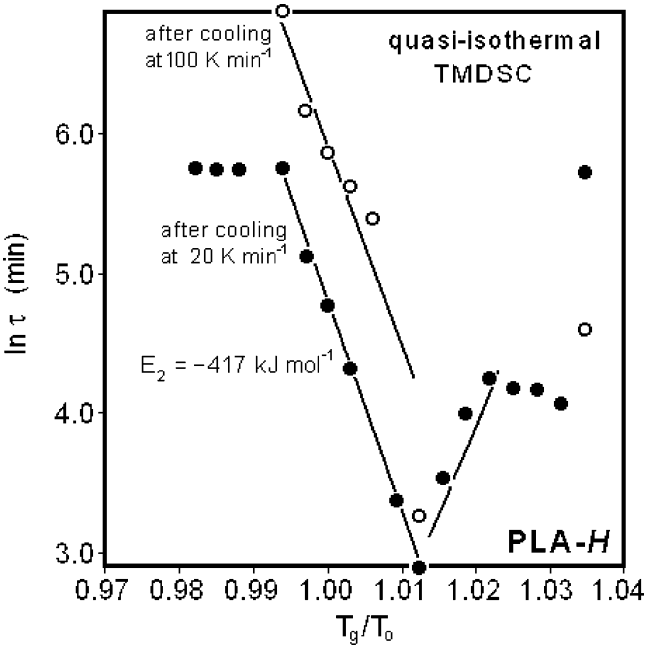

Figure 11. Logarithm of the relaxations times of aging from C_p(reversing) vs the reciprocal of T_0 normalized to T_g, evaluated by quasi-isothermal TMDSC, as in the examples given in Figure 10.

Next, isothermal aging of PLA-*H* was followed in the time domain with quasi-isothermal measurements at successively lower temperatures. Each sample was first heated to 373 K and then quenched inside the calorimeter to the quasi-isothermal base temperatures, T_0. Figure 10 shows two examples of the C_p(reversing) vs time in the glass transition range, but above T_g. The data were fitted to a double exponential. For the chosen time interval $\tau_2 = \tau_1$, and an amount of truly reversible heat capacity, C_{inf} remains at long times with values intermediate between the C_p(liquid) and C_p(solid). It is surprising that τ at the lower temperature is considerably less.

Figure 11 shows a plot of the logarithm of τ from Figure 10 obtained at successively lower temperatures vs the reciprocal of T_0. The two sets of data were generated by measurement after cooling from above the glass transition at 20 and 100 K min^{-1} instead of uncontrolled quenching. The T_g used to normalize T_0 was 329.2 K for both sets of experiments. Note the surprising changes in activation energy, mentioned already in the description of Figure 10. Below T_g, the decreasing trend of the relaxation time with T_0 reverses, as one would expect, and the slope changes to a positive value, as expected when approaching the glassy state.

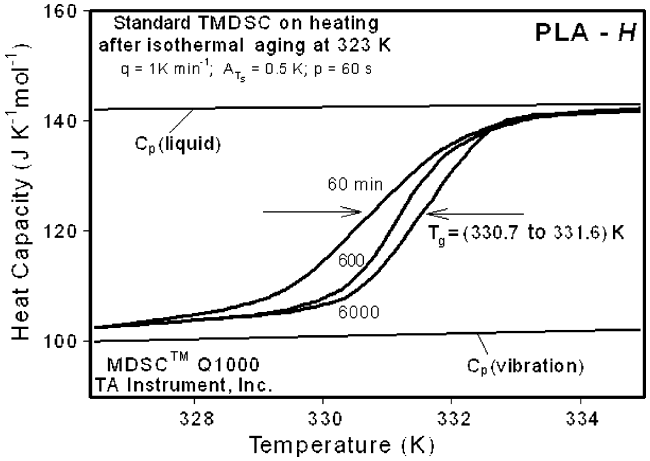

Figure 12. Plots of C_p(reversing) by standard TMDSC of PLA-*H* on heating after different lengths of isothermal aging below the glass transition, at 323 K ($\langle q \rangle$ = 1.0 K min^{-1}, p = 60 s, and A_{T_s} = 0.5 K).

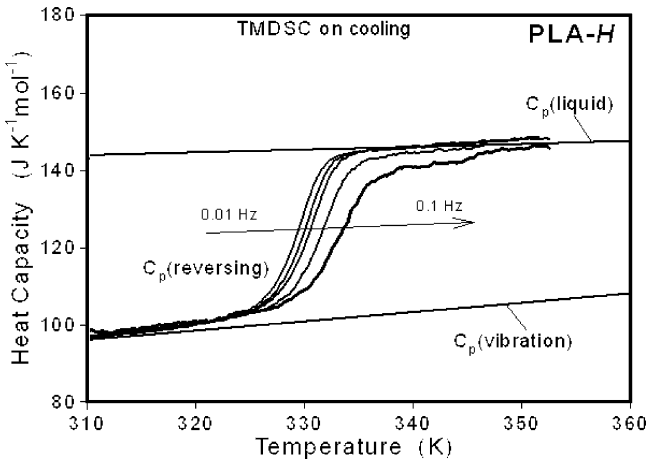

Figure 13. Plots of C_p(reversing) by TMDSC of PLA-*H* on cooling at ω and amplitudes such that $A_{T_s}\omega = \pi/100$ K s^{-1} = 1.88 K min^{-1} for every run ($\langle q \rangle$ = 0.1 K min^{-1}, p = 100−10 s, and A_{T_s} = 0.05−0.5 K).

Figure 12 shows examples of C_p(reversing) of PLA-*H* after isothermal aging below the glass transition at 323 K, followed by TMDSC with $\langle q \rangle$ = 1.0 K min^{-1}, A_{T_s} = 0.5 K, and p = 60 s. The reversing C_p of amorphous PLA-*H* are presented after isothermal aging for 1, 10, and 100 h. A curve of 20 min aging is not sufficiently separated from the 60 min data to be shown in the graph.

Figure 13 displays C_p(reversing) on cooling for different ω. The samples were cooled from 373 to 283 K with an underlying cooling rate of 0.1 K min^{-1}, A_{T_s} = 0.05−0.5 K, and p = 100−10 s. For each sample A_{T_s} was chosen such that the maximum rate cooling was $A_{T_s}\omega = \pi/100$. Based on Figure 13, the activation energy E_a in the glass transition region is 554.9 kJ mol^{-1}.

4. Discussion

4.1. Heat Capacity. Thermal analyses of amorphous and semicrystalline polymers by adiabatic calorimetry,

DSC, and TMDSC allow to separate and evaluate thermodynamic and kinetic processes within the regions of glass and melting transitions. In the solid state (below the glass and melting transition) the heat capacity is mainly caused by the vibrational motion with much faster time scales than in thermal analysis. Above the transitions, some of these vibrations have changed to large-amplitude motion, which in polymers is mainly conformational, and develops from torsional vibrations. In the transition-free temperature ranges, thermal analysis techniques yield the reversible thermodynamic heat capacity [$= (\partial H/\partial T)_{p,n}$]. As an arrested state, the heat capacity of the glass can also be treated as a thermodynamic heat capacity. Naturally, the instrument lags caused by thermal conductivity are assumed to be eliminated properly, a fundamental condition for every quantitative thermal analysis. In the range of first-order transitions, such as melting and crystallization, latent heats [$(= (\partial H/\partial n)_{p,T}$] are absorbed or released. These processes may be irreversible and also sufficiently slow to stretch over a temperature range during thermal analysis and are then added to the measured "apparent" heat capacity: $(dH/dT) = (\partial H/\partial T)_{p,n} + (\partial H/\partial n)_{p,T}(dn/dT)$, where (dn/dT) is linked to the kinetics of phase transitions. Thermal analysis provides the rate of change with temperature (dT/dt) and the heat-flow rate (dH/dt) for the study of the time dependence. Similarly, in the glass transition range, the response of the sample to a change in temperature may yield exothermic or endothermic enthalpy relaxations, including the hysteresis or aging. The first step which can lead to a separation of the components of the apparent C_p is to establish the thermodynamic C_p of the solid and liquid as baseline for further discussion. The baselines for the C_p of the glass and liquid are seen in Figures 2−7, 12, and 13. The TMDSC of many first-order transitions of polymers have been summarized recently,[17] and the glass transitions of amorphous polystyrene and semicrystalline poly(ethylene terephthalate) have also been analyzed in detail.[27−31]

4.2. Adiabatic Calorimetry and Standard DSC. Figure 1 illustrates the qualitative DSC traces. At the glass transition one observes a small hysteresis, and the melting region is obvious from the large endothermic peak. The heat capacity of these samples can already be quantified in the temperature regions outside of the transitions by the usual corrections for asymmetry and calibration with sapphire and extension of the data by adiabatic calorimetry to low temperature.[17]

Figure 2 shows the fit of the quantitative analysis of the two PLAs of Figure 1 in the frame of C_p(vibration) and C_p(liquid). The C_p(vibration) is based on low-temperature heat capacity measured by adiabatic calorimetry, while C_p(liquid) results from the DSC of amorphous PLA-*H*. Figure 2 shows good agreement with the measured C_p below the glass transition of the solid PLAs. The C_p is fully accounted for by vibrational motion. The semicrystalline PLA-*L* shows a ΔC_p of 14.8 J K^{-1} mol^{-1} at a T_g of 333 K, which corresponds to an amorphous content of 34%. With such analyses of ΔC_p at T_g and the measured heats of fusion, ΔH_f, for samples of different w_c, the heat of fusion for 100% crystalline PLA was extrapolated to be 6.55 ± 0.02 kJ mol^{-1} (91 ± 3 J g^{-1}) at T_m^o, estimated to be 480 K. Next, $w_c(T)$ was calculated for the semicrystalline PLA-*L* in the melting region, as presented previously, and indicated by the thin line in Figure 2. [2] More details about these transitions are available from TMDSC and are discussed next.

4.3. Glass Transitions and First-Order Transitions Studied by TMDSC. Good agreement of C_p(reversing) with the baselines of Figure 2 is achieved for all PLA samples for the glassy and liquid heat capacities in Figures 5−7, 12, and 13. The step in heat capacity at the glass transition of amorphous PLA-*H* by quasi-isothermal TMDSC is presented in Figure 3. Within the glass transition region C_p(reversing) depends on ω, as discussed in section 4.4 with Figure 13. The C_p(revering) of eq 3 does not show hysteresis contributions as seen in the C_p by standard DSC in Figures 2, 6, and 7 and discussed in more detail in section 4.4 based on Figures 7 and 8.

When using TMDSC with increasing $\langle q \rangle$, Figure 4 reveals small changes in C_p(reversing) in the glass transition range from the quasi-isothermal TMDSC of Figure 3. Only when $\langle q \rangle$ approaches zero are the data of Figure 3 reached. This behavior was discovered earlier in a TMDSC study of atactic polystyrene[27] and was later seen for amorphous poly(ethylene terephthalate).[38] The reasons for these differences are the following: (1) a small shift in the reversing C_p due to interaction between the time scales of modulation and $\langle q \rangle$, (2) a distortion of C_p(reversing) due to different enthalpy relaxations on heating and cooling, and (3) the fluctuation in the C_p(reversing) and C_p(nonreversing) due to a small shift in the frequency of heat-flow-rate modulation relative to ω. For these reasons, quantitative data on C_p(reversing) can only be obtained by quasi-isothermal TMDSC. Furthermore, the total C_p is best taken from a standard DSC.

In Figure 5 sharper glass transitions are observed for amorphous than for semicrystalline PLA, resulting from stress transfer through the points of molecular decoupling between phases. [39] The amorphous fractions calculated from ΔC_p at T_g in the semicrystalline sample (Figure 5) and on cold crystallization (Figure 6) when added to the w_c from the heat of fusion account for all polymer; i.e., none of the analyzed PLA-*L* samples contain a rigid amorphous fraction (RAF).[17]

The cold crystallization of PLA-*L* in Figures 5 and 6 starts at about 355 K and is irreversible. The four to five points between the C_p(liquid) and the dashed line for $w_c = 51\%$ are determined by the rate of crystallization and could have been used for its determination.[40] A $w_c = 51\%$ is reached by the amporphous PLA-*L* heated at 2.0 K min^{-1} (Figure 6) and compares to $w_c = 66\%$ for the isothermally crystallized sample (Figures 2 and 5). On the DSC of amorphous PLA-*L* at the much faster 20 K min^{-1}, cold crystallization is still not completely suppressed, as is seen by the exotherm at ≈400 K and the subsequent small melting peak. All semicrystalline samples show broad melting ranges, starting at ≈370 K (Figures 5 and 6). At lower temperatures, the latent heat contribution to dH/dT is reversible, but it becomes very small within the major melting peak. The cold-crystallized sample has the higher reversing melting peak, as also observed for many other macromolecular crystals.[17] More details about the melting region of TMDSC will be reported in the future.

4.4. Hysteresis and Aging in the Glass Transition Range of Amorphous PLA-*H*. The C_p of PLA-*H* in Figures 7 and 8a illustrates the hysteresis in the glass transition range. Overall, there are two major overlapping effects, which complicate the change from solid to

liquid C_p at the glass transition. First, there is the endothermic peak, approximately separated in Figure 8c, and second, there is a change of C_p(reversing) as illustrated in Figure 8b. A smaller, but still important, effect is caused by the aging which occurs as an exotherm during heating, starting below T_g and continuing into the temperature range of the endothermic hysteresis. In Figure 9a it gives an explanation why DSC on cooling (open circles) and TMDSC on heating (filled circles) do not approach at high cooling rates. Similarly, the enthalpy relaxation in Figure 9b does not reach zero, as one might expect when not considering this effect.

The separation of the reversing and irreversible processes at the glass transition in Figure 8b,c is only approximate, as mentioned above. As noted in section 2.4, a detailed model is necessary to fully separate the thermodynamic heat capacity from the total measurement. The earlier discussion of this topic with a first-order kinetics fitted to a simple hole model, however, could show that the error in Figure 8b,c is small.[37] No further discussion is given here.

Figure 8b documents that the more annealed PLA-*H* has a higher T_g, while on cooling, it has a lower T_g (open circles in Figure 9a). Figure 4, furthermore, shows a narrower transition range on heating rather than on cooling. This was linked already some years ago to the cooperative nature of the glass transition when studying polystyrene by dynamic differential thermal analysis.[41] On heating, the unfreezing of the high-energy configurations of more aged samples begins at higher temperature. On cooling, configurations which need bigger cooperative rearrangements relax to lower temperatures and produce annealed (aged) samples of lower enthalpy, as seen in Figure 9a.

The degree of aging of a glass is not detectable by C_p because all solids have practically the same C_p, as seen in Figure 7. The enthalpy, thus, must be evaluated by integration of C_p to the equilibrium liquid. The samples with a larger integral have a lower enthalpy and are more aged. One, furthermore, must recognize that even glasses with identical enthalpies may be different. It was shown in the past, for example, that glasses of low enthalpy can be produced on slow cooling or quenching from high pressure.[42] Such different glasses have a different hysteresis behavior. It is of importance to recognize that a glass which is not in equilibrium needs additional internal variables for its description. These variables are arrested below T_g and can relax on heating with different kinetics.[43] Even volume and enthalpy may follow different kinetics on unfreezing.[42]

The evaluation of the relaxation time, τ, within the glass transition region measured by quasi-isothermal TMDSC supports the suggestion that an aged sample needs more cooperativity, as illustrated in Figures 10 and 11. At higher temperatures ($T_g/T_0 < 0.995$) and on a slow approach to T_0 an almost constant τ is seen as the samples may have be close to H(liquid). This is followed by a linearly decreasing (!) ln τ until T_g/T_0 is 1.01; still, C_p(reversing) decreases properly with increasing time, i.e., the sample approaches a state of lower enthalpy. Perhaps, at lower temperatures one selectively assesses the increasingly smaller clusters of cooperatively freezing high-energy configurations (holes). These, then, would have increasingly shorter relaxation times, as can be seen from the examples in Figure 10. At lower temperatures, beyond $T_g/T_0 = 1.01$, the logarithm of the relaxation times increases with practically the same slope, but which is now positive, signaling a constant cluster size. More details of a description by the commonly applied empirical equations in the literature and a new approach related to changes of conformational C_p and its cooperativity in the glass transition region are the subjects in a forthcoming study.

After isothermal aging, T_g derived from C_p(reversing) shifts to higher temperatures, as illustrated in Figure 12. The difference between T_g after aging for 1.0−100 h is only about 1 K, but differences in the shapes of C_p(reversing) are significant. Similar to Figure 8b, this is evidence of the cooperative nature of the glass transition, high-energy conformations devitrify in a aged sample at higher temperature. The different shapes of the reversing C_p at T_g may be related to different correlation lengths or packing parameters during the cooperative process.

The changes with frequency of C_p(reversing) at identical heating-rate profiles of the modulation and a fixed $\langle q \rangle$ of −0.1 K min^{-1} are displayed in Figure 13. On increasing the frequency from 0.01 to 0.1 Hz, the sample shows an increase of T_g by ≈5 K. Such increase in T_g is also seen by DSC when changing q from −0.1 to −20 K min^{-1} (bottom half of Figure 9a). The glasses of higher T_g have higher enthalpies. These two observations contrast the C_p(reversing) of Figure 8b. At a given ω and $\langle q \rangle$, the samples with higher enthalpy in the glassy state have lower T_gs on heating. The enthalpy difference is found in the irreversible hysteresis peak.

The activation energy derived from the data of Figure 13 is 559 kJ mol^{-1}, of expected order of magnitude.[41] Additional results and an extensive discussion are planned for the future.

5. Conclusions

A quantitative study of the glass transitions of amorphous and semicrystalline poly(lactic acid)s by TMDSC and DSC permits approximate separation of the thermodynamic and kinetic processes in the glass transition region. Thermodynamic C_p, hysteresis, and aging effects caused by the freezing and unfreezing of large-amplitude motion cause overlapping effects and have been approximately separated. Using TMDSC, the reversing and nonreversing effects in the glass transition and melting and crystallization regions of PLA could be studied. The cold crystallization of PLA-*L* was seen to be irreversible, as is the major part of melting. The reversing melting of isothermally crystallized PLA-*L* is close to 100% from 375 to 420 K and becomes very small inside the major melting peak. The enthalpy relaxations in the glass transition region of PLA-*H* were found to be fully irreversible, although a certain, small amount of the reversing effect derived from the first harmonic is lost due to higher harmonics generated and wrong assignment due to constant contributions to C_p and frequency shifts.

The reversing heat capacities after isothermal and nonisothermal aging result in glasses with lower enthalpy, which show shifts of the glass transition temperature to higher temperatures on subsequent heating. Direct measurement of the relaxation time of aging by quasi-isothermal TMDSC shows a non-Arrhenius behavior in C_p(reversing) when approaching the glass transition temperature. Only below T_g does the logarithm of the relaxation time increase linearly.

Acknowledgment. This work was supported by Cargill Dow LLD, Chem. Co. and the Division of Materials Research, National Science Foundation, Polymers Program, Grant DMR-0312233. Use of some of equipment and laboratory space was provided by the Division of Materials Sciences and Engineering, Office of Basic Energy Sciences, U.S. Department of Energy at Oak Ridge National Laboratory, managed and operated by UT-Battelle, LLC, for the U.S. Department of Energy, under Contract DOE-AC05-00OR22725. A supplemental grant by the Scholarly Activities Research Incentive Funds, SARIF, of the University of Tennessee is also acknowledged.

References and Notes

(1) Wunderlich, B. Heat capacity of polymers. In Cheng, S. Z. D., Ed.; *Handbook of Thermal Analysis and Calorimetry*; Elsevier Science: Amsterdam, 2002; Vol. 3.
(2) Pyda, M.; Bopp, R. C.; Wunderlich, B. *J. Chem. Thermodyn.* **2004**, *36*, 731.
(3) Abe, H.; Kikkawa, Y.; Inoue, Y.; Doi, Y. *Biomacromolecules* **2001**, *2*, 1007.
(4) Gorlotta, D. J. *Polym. Environ.* **2001**, *9*, 63.
(5) Vainiopaa, S.; Rokkanem, P.; Tormala, P. *Prog. Polym. Sci.* **1989**, *14*, 679.
(6) Baratian, S.; Hall, E. S.; Lin, J. S.; Xu, R.; Runt, J. *Macromolecules* **2001**, *34*, 4857.
(7) Kalb, B.; Penings, A. J. *Polymer* **1980**, *21*, 607.
(8) Kanchanasopa, M. Solid-state Structure and Dynamics of Lactide Copolymers and Blends. DMSE, Dissertation, Pennsylvania State University, 2004.
(9) Huang, J.; Lisowski, M. S.; Runt, J.; Hall, E. S.; Ken, R. T.; Buehler, N.; Lin, J. S. *Macromolecules* **1998**, *31*, 2593.
(10) Loomis, G. L.; Murdoch, J. R.; Gardner, K. H. *Polym. Prepr.* **1990**, *31* (2), 55.
(11) Witzke, D. R. Introduction to Properties Engineering and Prospects of Polylactide Polymers. UMI, Dissertation, Michigan State University, East Lansing, MI, 1997.
(12) Hill, V. L.; Passerini, N.; M.; Craig, D. Q.; Vickers, M.; Anwa, J.; Feely, L. C. *J. Therm. Anal. Calorim.* **1998**, *54*, 674.
(13) Penning, J. P.; Dijstra, H.; Pennings, A. J. *Polymer* **1993**, *34*, 942.
(14) Sarasua, J. R.; Prud'homme, R. E.; Wisniewski, M.; Le Borgne, A.; Spassky, N. *Macromolecules* **1998**, *31*, 3895.
(15) Cohn, D.; Hotovely-Salomon, A. *Polymer* **2005**, *46*, 2068.
(16) Wunderlich, B. *Thermal Analysis of Polymeric Materials*; Springer-Verlag: Berlin, 2005.
(17) Wunderlich, B. *Prog. Polym. Sci.* **2003**, *28*, 383.
(18) Schick, C. Temperature Modulated Differential Scanning Calorimetry (TMDSC)—Basics and Applications to Polymers. in Cheng, S. Z. D., Ed.; *Handbook of Thermal Analysis and Calorimetry*; Elsevier Science: Amsterdam, 2002; Vol. 3.
(19) McKenna, G. B.; Simon, S. L. The glass transition: its measurements and underlying physics. In Cheng, S. Z. D., Ed.; *Handbook of Thermal Analysis and Calorimetry*; Elsevier Science: Amsterdam, 2002; Vol. 3.
(20) Wunderlich, B. *Pure Appl. Chem.* **1995**, *67*, 1019.
(21) Pyda, M. Ed.; *The ATHAS Data Bank*, 2005: http://web.utk.edu/~athas/databank.
(22) Pyda, M.; Wunderlich, B. *Macromolecules* **1999**, *32*, 2044.
(23) Pyda, M. *J. Polym. Sci., Part B: Polym. Phys.* **2001**, *39*, 3038.
(24) Pyda, M. *Macromolecules* **2002**, *35*, 4009.
(25) Pyda, M. In Lorinczy, D., Ed.; *The Nature of Biological Systems as Revealed by Thermal Methods*; Kluwer Academic Publisher: Amsterdam, 2004.
(26) Reading, M., Ed.; *Basic Theory and Practice for Modulated Temperature Differential Scanning Calorimetry (MTDSC)*; Kluwer Academic Publishers: Dordrecht, The Netherlands, 2005.
(27) Boller, A.; Schick, C.; Wunderlich, B. *Thermochim. Acta* **1995**, *266*, 97.
(28) Boller, A.; Okazaki, I.; Wunderlich, B. *Thermochim. Acta* **1996**, *284*, 1.
(29) Wunderlich, B.; Okazaki, I. *J. Therm. Anal.* **1997**, *49*, 57–70.
(30) Okazaki, I.; Wunderlich, B. *J. Polym. Sci., Part B: Polym. Phys.* **1996**, *34*, 2941.
(31) Thomas, L. C.; Boller, A.; Okazaki, I.; Wunderlich, B. *Thermochim. Acta* **1997**, *291*, 85.
(32) Reading, M. *Trends Polym. Sci.* **1993**, *8*, 248.
(33) Wunderlich, B.; Jin, Y.; Boller, A. *J. Thermochim. Acta* **1994**, *238*, 277.
(34) Turi, E., Ed.; *Thermal Characterization of Polymeric Materials*, 2nd ed.; Academic Press: New York, 1997.
(35) Kamasa, P.; Merzlyakov, M.; Pyda, M.; Pak, J.; Schick, C.; Wunderlich, B. *Thermochim. Acta* **2002**, *392/393*, 195.
(36) Pyda, M.; Kwon, Y. K.; Wunderlich, B. *Thermochim. Acta* **2001**, *367/368*, 217.
(37) Wunderlich, B.; Boller, A.; Okazaki, I.; Kreitmeier, S. *J. Therm. Anal.* **1996**, *47*, 1013.
(38) Wunderlich, B.; Boller, A.; Okazaki, I.; Ishikiriyama, K. *Thermochim. Acta* **1997**, *304/305*, 125.
(39) Wunderlich, B. *J. Polym. Sci., Part B: Polym. Phys.* **2004**, *42*, 1275.
(40) Toda, A.; Arita, T.; Tomita, C.; Hikosaka, M. *Polym. J.* **1999**, *31*, 790.
(41) Wunderlich, B.; Bodily, D. M.; Kaplan, M. H. *J. Appl. Phys.* **1964**, *35*, 95.
(42) Weitz, A.; Wunderlich, B. *J. Polym. Sci., Polym. Phys. Ed.* **1974**, *12*, 2473.
(43) Baur, H. *Thermophysics of Polymers, I, Theory*; Springer: Berlin, 1999.

MA051611K